Supporting Information

Metal-Organic Frameworks in Seconds *via* Selective Microwave Heating

Andrea Laybourn,[a,b] Juliano Katrib,[b] Rebecca S. Ferrari-John,[b] Christopher G. Morris,[a,c] Sihai Yang,[a,c] Ofonime Udoudo,[b] Timothy L. Easun,[a,d] Chris Dodds,[b] Neil R. Champness,[a]* Samuel W. Kingman[b]* and Martin Schröder[a,c]**

a *School of Chemistry, University of Nottingham, Nottingham NG7 2RD, UK*
b *Faculty of Engineering, University of Nottingham, Nottingham NG7 2RD, UK*
c *School of Chemistry, Oxford Road, University of Manchester, Manchester M13 9PL, UK*
d *School of Chemistry, Main Building, Cardiff University, Park Place, Cardiff, CF10 3AT, UK*

Contents

1. Energy calculations and experimental values

Table S1: Thermo-physical properties of water for energy calculations.

Mass of water (g) m_L	Specific heat capacity of water (J/g.K)[a] C_p	Change in temperature (°C)[b] ΔT	Latent heat of vaporization of water (J/g) L_v	Mass of vaporized water (g) m_v
6.7	4.2[1]	210	2260[2]	6.7

[a]C_p at 100 °C for liquid water. The pressure of this system varies with temperature, and therefore the value used here is an estimate of the minimum energy required for bulk temperature rise. [b]With a start temperature of 10 °C.

Using values from Table S1 above, the energy required to heat water is given by equation 1 below:

$$\left((m_L \times C_p \times \Delta T) + \left(L_v \times m_v\right)\right) \qquad \text{Equation 1}$$

Therefore a reaction temperature of 220 °C requires 21 kJ of energy (or 56 kJ per mole of water).

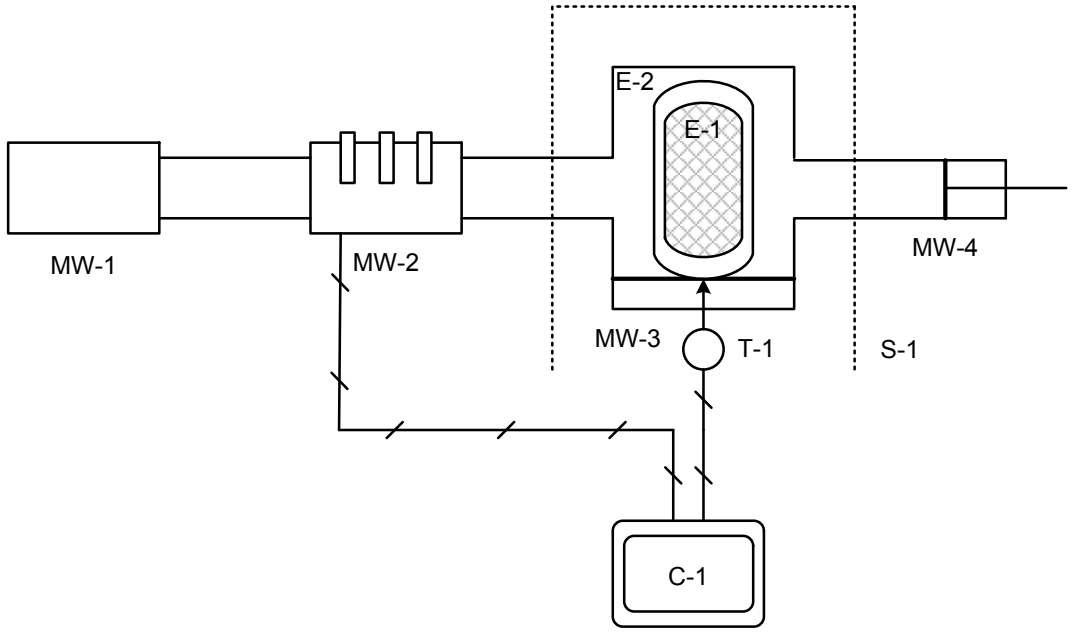

Figure S1: Schematic of purpose-built single mode microwave system. Labels are assigned in Table S2 below.

Table S2: Labels for purpose-built single mode microwave system shown in Scheme S1.

Label	Component
C-1	PC controller
E-1	Teflon cup for microwavable acid digestion vessel (Parr Instruments)
E-2	Outer section of microwavable acid digestion vessel (Parr Instruments)
MW-1	Microwave generator
MW-2	Automatic 3-stub tuner
MW-3	Microwave applicator/cavity section
MW-4	Sliding short
S-1	Lexan shield (blast-safe)
T-1	Optris CT IR sensor

2. Synthesis of MIL-53(Al)*ta* in 4.3 seconds

Chemicals: $Al_2(SO_4)_3.18H_2O$ was purchased from Acros Organics. Terephthalic acid was purchased from Alfa. All chemicals had a purity of 97% or greater and were used as received. The reaction mixture was treated with an applied power (from the generator) of 4.0 kW for 4.3 seconds. The average absorbed power and total absorbed energy into the reaction mixture during this time were recorded as 3.8 kW and 16.4 kJ (or 44.1 kJ mol^{-1} based on water), respectively. *CAUTION: heating above 4.3 seconds under these conditions leads to violent expulsion of the reactants due to excessive internal pressure*. After microwave irradiation, the reaction mixture was allowed to cool and the resulting white powder recovered by filtration, washed with deionised water (*ca.* 10 mL x 3) and dried in air. The yield of MIL-53(Al)*ta* was 62 mg (30 %) as determined by thermogravimetric analysis based on Al utilisation and the product $[Al(OH)(O_2C{-}C_6H_4{-}CO_2)]\cdot(H_2BDC)_n$. Removal of H_2BDC inside the pores of MIL-53(Al)*ta* by calcining the powder in a tube furnace at 330 °C for 7 days gave the open phase structure MIL-53(Al)*op* ($[Al(OH)(O_2C{-}C_6H_4{-}CO_2)]$) with a surface area of 285 m^2g^{-1} and a Type I N_2 isotherm (Figures S6 and S7).

Table S3: Average data for microwave heating experiments conducted at an energy of *ca.* 19 kJ (or 51 kJ mol^{-1} based on water).

Average power absorbed by reaction mixture (W)[a*]	Irradiation time (s)[a#]	Energy absorbed by reaction mixture (kJ/mol)[a,c#]	Energy absorbed by reaction mixture (kJ)[a#]	Yield of MIL-53(Al)*op* (%)[b#]	Yield of MIL-53(Al)*ta* (%)[b#]	Yield of AlN (%)[b#]
269 ± 2	71.7 ± 0.5	51.9 ± 0.3	19.3 ± 0.1	15.9 ± 7.0	22.2 ± 10.5	11.7 ± 6.2
359 ± 8	53.3 ± 1.5	51.4 ± 2.4	19.1 ± 0.9	18.8 ± 6.3	24.3 ± 8.1	20.1 ± 7.6
448 ± 1	42.5 ± 0.6	51.1 ± 0.8	19.0 ± 0.3	18.9 ± 2.4	26.2 ± 4.6	18.3 ± 1.7
532 ± 18	35.5 ± 0.6	50.8 ± 2.4	18.9 ± 0.9	29.0 ± 5.2	34.5 ± 5.9	36.0 ± 7.3
682 ± 4	28.0 ± 1.0	51.4 ± 1.6	19.1 ± 0.6	36.8 ± 4.9	46.7 ± 5.6	39.5 ± 6.6
891 ± 4	22.0 ± 0.9	52.7 ± 1.6	19.6 ± 0.6	29.1 ± 6.2	34.0 ± 6.8	36.2 ± 9.0
945 ± 11	20.3 ± 0.2	51.6 ± 1.3	19.2 ± 0.5	32.1 ± 6.1	39.0 ± 6.4	37.2 ± 8.6
1314 ± 27	15.0 ± 1.0	53.0 ± 2.2	19.7 ± 0.8	29.2 ± 3.4	33.6 ± 4.4	41.1 ± 5.1
1739 ± 44	10.4 ± 0.3	48.7 ± 1.3	18.1 ± 0.5	28.5 ± 6.5	33.9 ± 7.3	36.4 ± 9.4
2762 ± 86	6.5 ± 0.7	48.7 ± 3.0	18.1 ± 1.1	31.2 ± 6.8	36.9 ± 9.2	40.2 ± 7.9
3819 ± 92	4.3 ± 0.4	44.1 ± 1.6	16.4 ± 0.6	30.2 ± 8.8	34.7 ± 9.9	38.9 ± 11.0

Values are given to [*]0 and [#]1 decimal places. [a] Each value represents an average of 3 experiments. [b] Each value represents an average of 9 values (3 experiments with yields calculated from TGA analyses run in triplicate). Errors are values ± one standard deviation. [c] Based on water.

3. Powder X-ray diffraction (PXRD) data

Diffraction patterns were recorded on a PANanalytical diffractometer with a $CuK_{\alpha 1}$ X-ray source (operating at 40kV and 40mA) and a PIXcel DKIW179H1 detector. Samples of MIL-53(Al)*op* were loaded on 5.1.0 silicon plates and diffraction recorded in the 2θ range of 5-55º. Relative crystallinity was determined using a previously reported method whereby the reciprocals of the full width half maximum (1/FWHM) for a selected peak are compared.[3] In this work the (110) reflection located at 2θ = 12.3° was chosen as this peak has considerable intensity and is uncrowded in all of the samples. A split pseudo-Voigt peak function was used to fit the peak owing to the asymmetry. The same instrument and mass of sample was used for all PXRD collections to ensure consistency in the contribution of instrumental peak broadening.

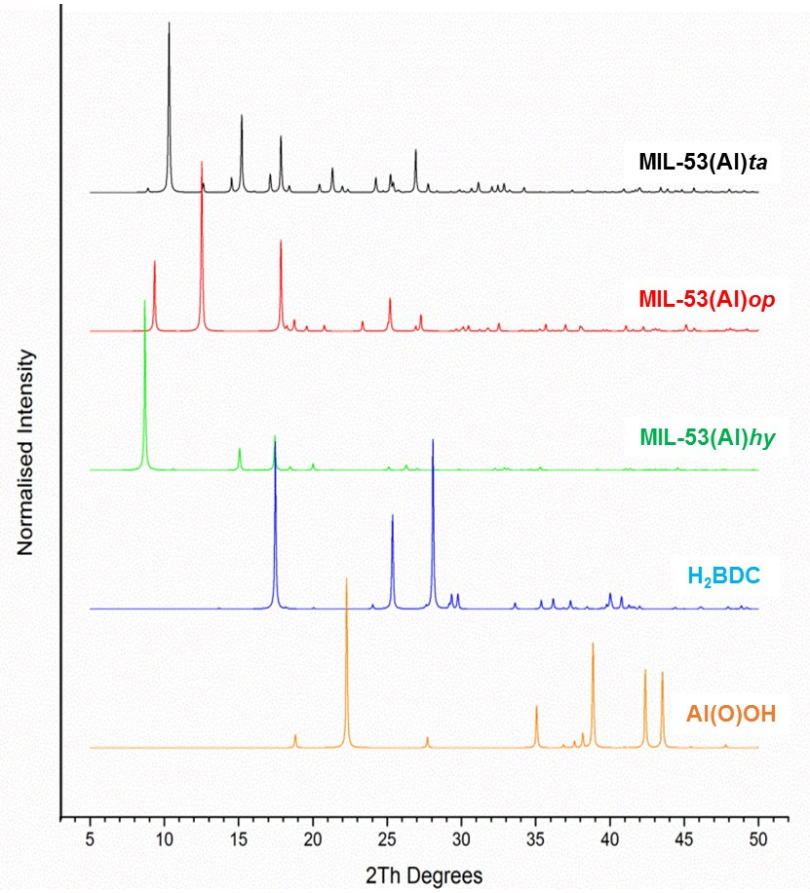

Figure S2: Simulated PXRD patterns of reported phases of MIL-53(Al), H_2BDC and γAlO(OH). The phases MIL-53(Al)*op* (CDS reference code SABVUN) and MIL-53(Al)*hy* (CDS reference code SABWAU) were first reported by Loiseau *et al*.[4] The MIL-53(Al)*ta* phase (CDS reference code SABVOH01) was reported by Vougo-Zanda *et al*.[5] H_2BDC (CDS reference code TEPHTH) was first reported by Bailey *et al*.[6] γ-AlO(OH) (ICSD collection code 59609) was reported by Bokhimi *et al*.[7] Simulated PXRD patterns were generated from CDS data using Mercury version 3.3.

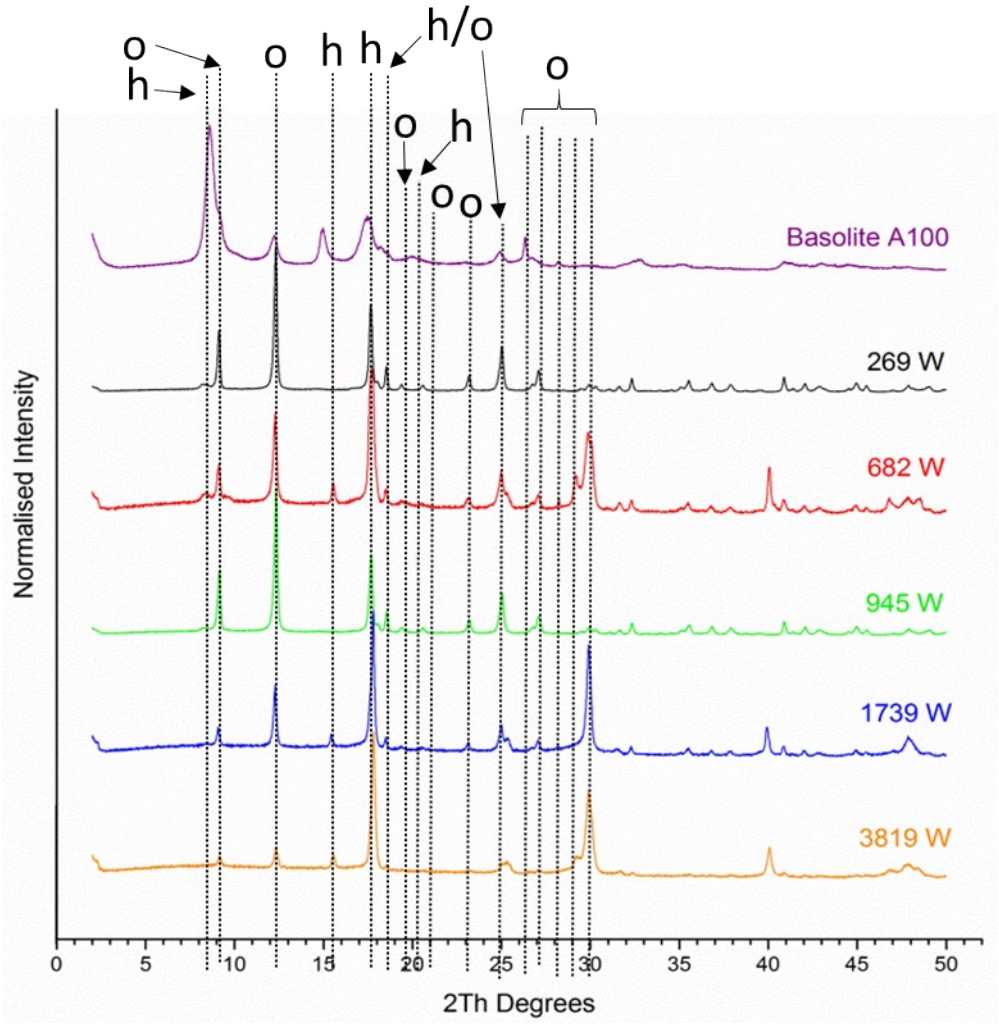

Figure S3: PXRD patterns of commercial material and products isolated from reactions at various microwave powers (inset) after calcination at 330 °C for 7 days. Calcination procedure adopted from Bayliss et al.[8] Owing to significant peak overlapping for MIL-53(Al)*ta* and MIL-53(Al)*op* phases it was not possible to compare PXRD patterns for mixtures recovered from reaction without prior calcination. Each PXRD pattern contains a mixture of MIL-53(Al)*op* (peaks labelled o) and MIL-53(Al)*hy* phases (peaks labelled h). Hydration of microwave-synthesised MIL-53(Al)*op* occurs upon atmospheric exposure after removal from the tube furnace.

Split pseudo-Voigt peak fitting

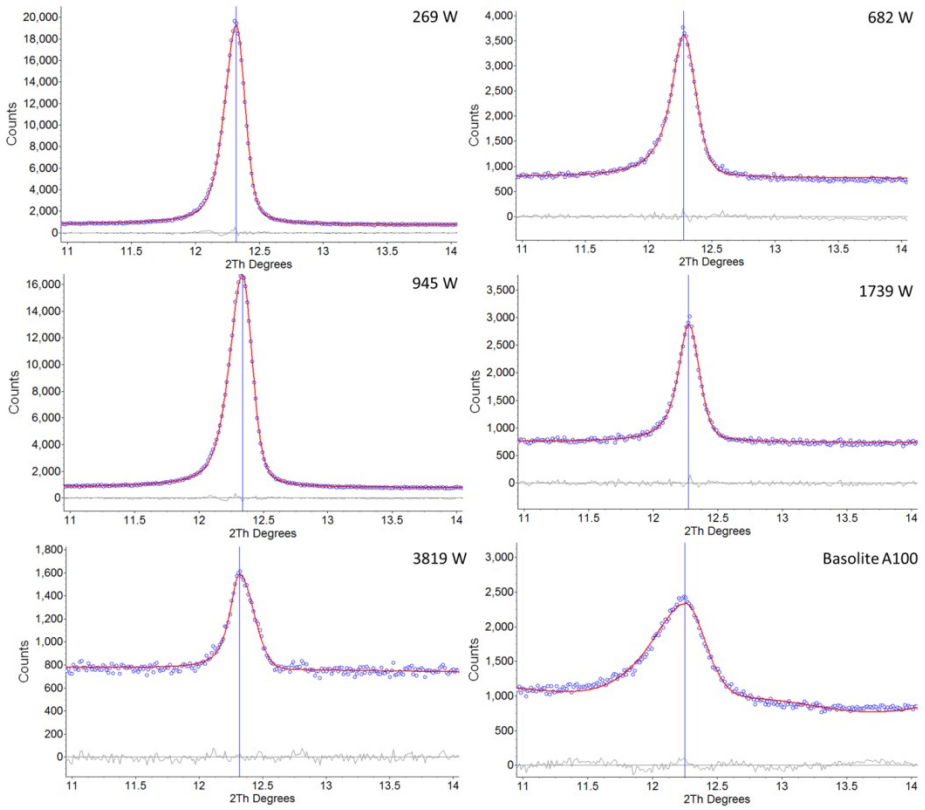

Figure S4: Peak fits of the (1 1 0) reflection of MIL-53(Al)*op* materials recovered at various powers and the commercial material (labelled inset). Blue open circles = experimental powder pattern; Red line = calculated peak profile; Grey line = difference.

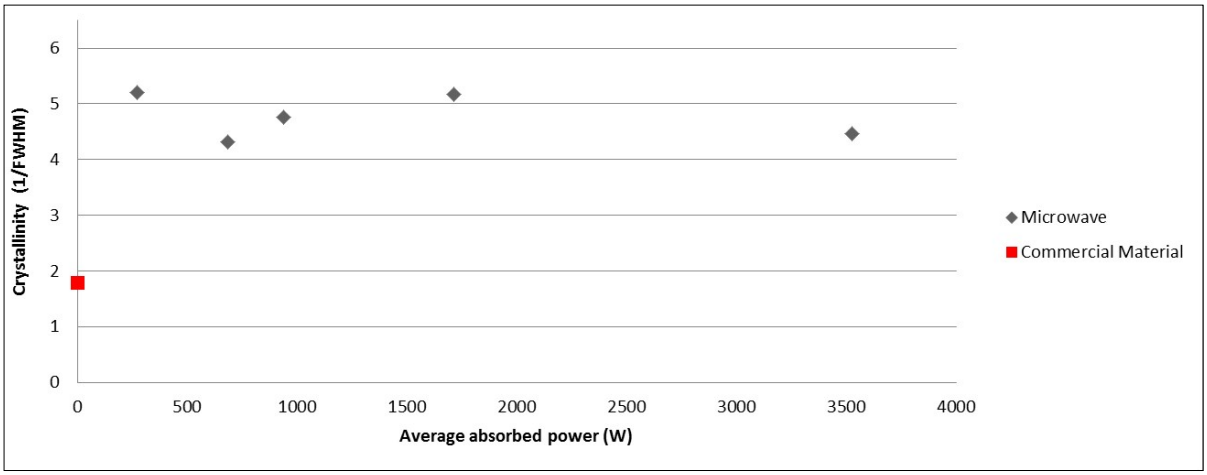

Figure S5. Plot of average absorbed power *vs.* relative crystallinity of MIL-53(Al)*op* materials (squares). The crystallinity was also determined for the commercial material, Basolite A100 (red square). Crystallinity is determined from 1/FWHM for PXRD peaks at the 110 reflections. (See Experimental section and Supporting Information for further details).

4. Gas sorption isotherms

Gas sorption analyses were performed on samples of MIL-53(Al)*op*. These were prepared by removal of terephthalic acid from the pores of MIL-53(Al)*ta* by calcining the material in a tube furnace at 330 °C for 7 days. Surface areas and pore size distributions for MIL-53(Al)*op* were measured by N_2 adsorption and desorption isotherms in the range 0.001 – 0.99 P/P_0 with 95 data points at 77.3 K using a Micromeritics 3-flex volumetric adsorption analyser. Samples were degassed at 120 °C for 15 h under vacuum (10^{-5} bar) before analysis. N_2 adsorption isotherms were analysed using Micromeritics MicroActive software and are plotted in Figures S6-S7 below. Data are summarised in Table 2 in the main text.

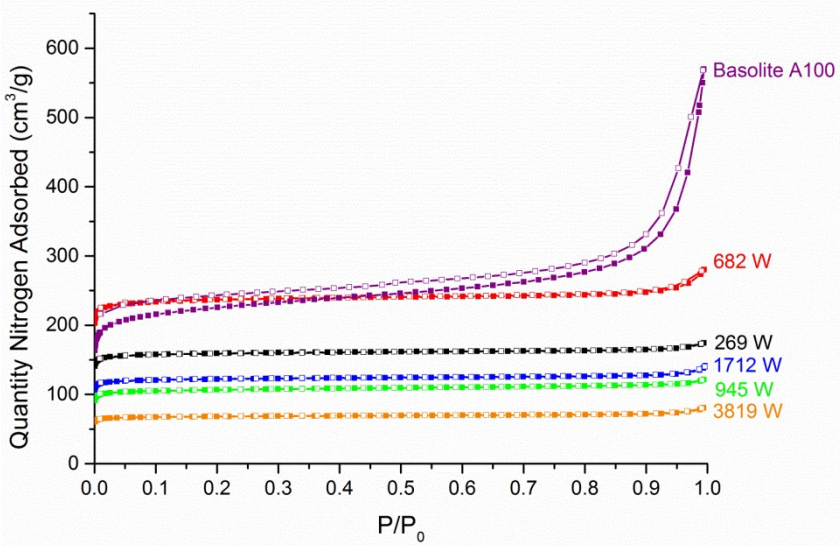

Figure S6: N_2 adsorption-desorption isotherms collected at 77 K for commercial material and for MIL-53(Al)*op* prepared *via* microwave heating at various powers (labelled inset). Adsorption (filled squares), desorption (hollow squares). Above 0.8 P/P_0 the commercial material shows significant adsorption and desorption owing to inter-particulate porosity. All materials prepared *via* microwave heating exhibit Type I isotherms[9] with little hysteresis, characteristic of a micro-porous material.

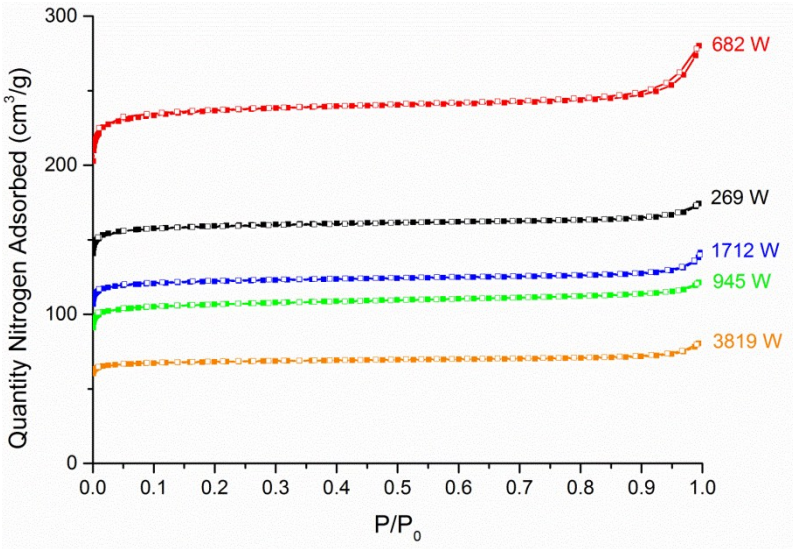

Figure S7: N_2 adsorption-desorption isotherms for MIL-53(Al)*op* materials prepared *via* microwave heating at various powers (labelled inset).

5. **Scanning electron microscopy (SEM) images and histogram plots**

High-resolution SEM images of MIL-53(Al)*ta* were collected using an FEI Quanta 600 scanning electron microscope equipped with a tungsten filament electron/energy source, two Bruker XFlash® 5030 energy dispersive X-ray spectrometers, a secondary electron detector and a backscatter electron detector. Samples were prepared on 10 mm aluminium stubs with an adhesive carbon tab, tapping the tab to remove any un-stuck sample. The samples of MIL-53(Al)*ta* samples were coated with a 2 nm layer of gold using a Polaron PS3 sputter coater, and imaging was conducted at a working distance of 13 mm using the secondary electron detector with an accelerating voltage of 25 kV. Frame captures of high resolution MIL-53(Al)*ta* morphologies were obtained using the AnalySIS image processing software manufactured by Olympus. Energy dispersive X-ray spectroscopy was used to distinguish between MOF crystals and residual terephthalic acid by confirming aluminium content. Crystals containing aluminium were grouped according to size and morphology. Crystal sizes were determined using the area of one face of the crystal, and crystals were grouped based upon morphology using the following characteristics:

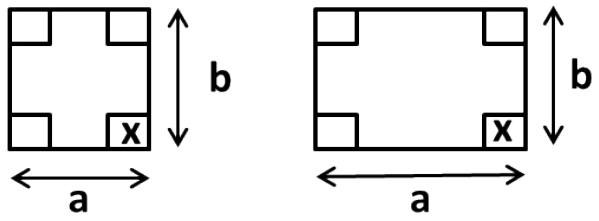

Cubes: all 90° angles plus a = b

Rectangles: all 90° angles plus a < 1.5b

Irregular shapes: contains less than four 90° angles

A total of 100 MIL-53(Al)*ta* crystal dimensions and morphologies were extracted using the measure function of the AnalySIS software and plotted according to size in histogram plots (see Figures S9-12). Exemplar SEM images are shown in Figure S8 below. Data are also summarised as a box and whisker plot in Figure 3 in the main text.

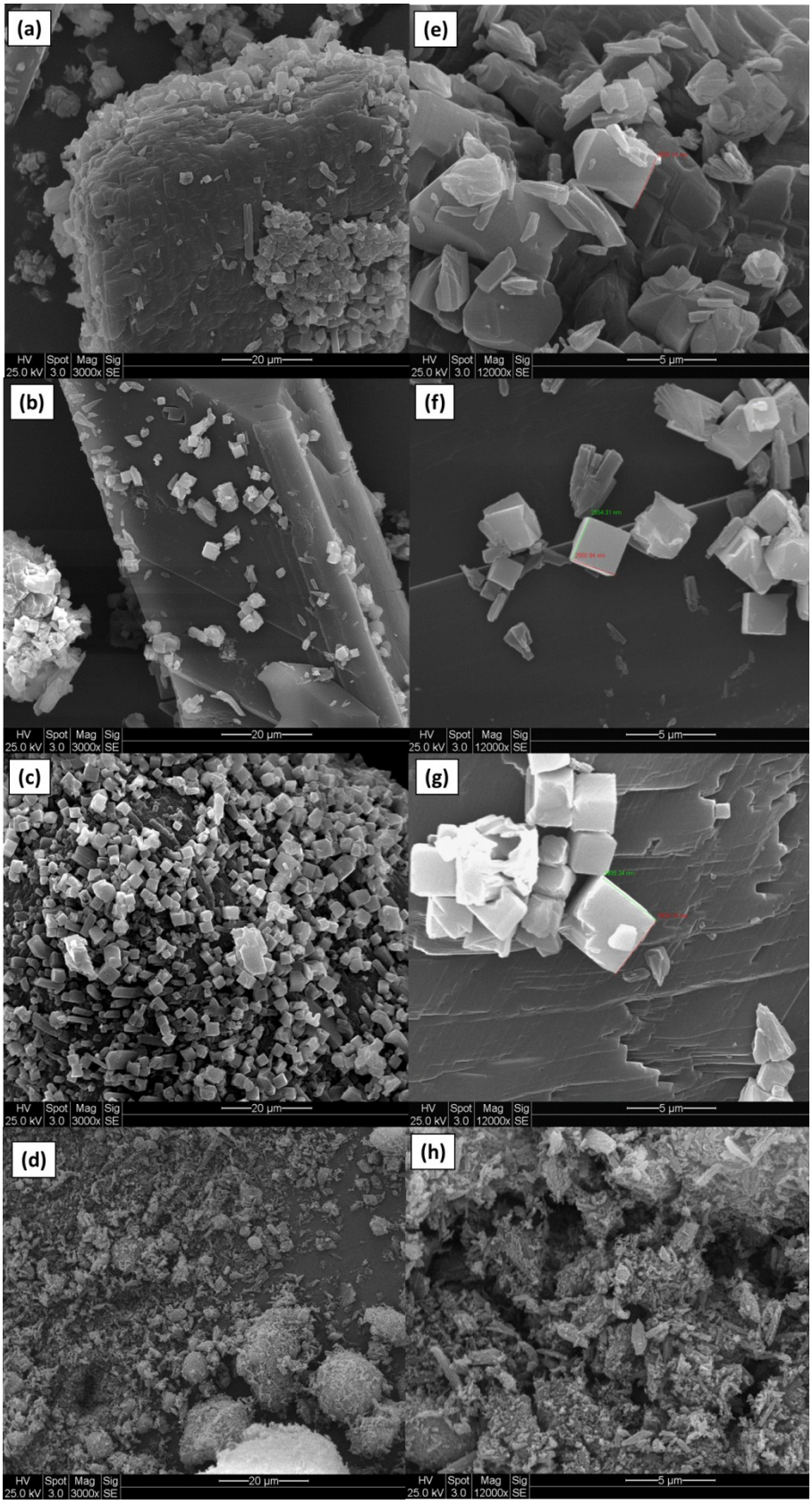

Figure S8: SEM images of MIL-53(Al)*ta* collected from reactions conducted at powers of 269 ± 2 (a, e), 682 ±4 (b, f) and 1739 ± 44 W (c, g) and the commercial material (Basolite A100, d and h). Scale bars of 20 µm (a-d) and 5 µm (e-h) are inset. Larger structures (particularly prominent in the background of a, b and g) correspond to unreacted H_2BDC.

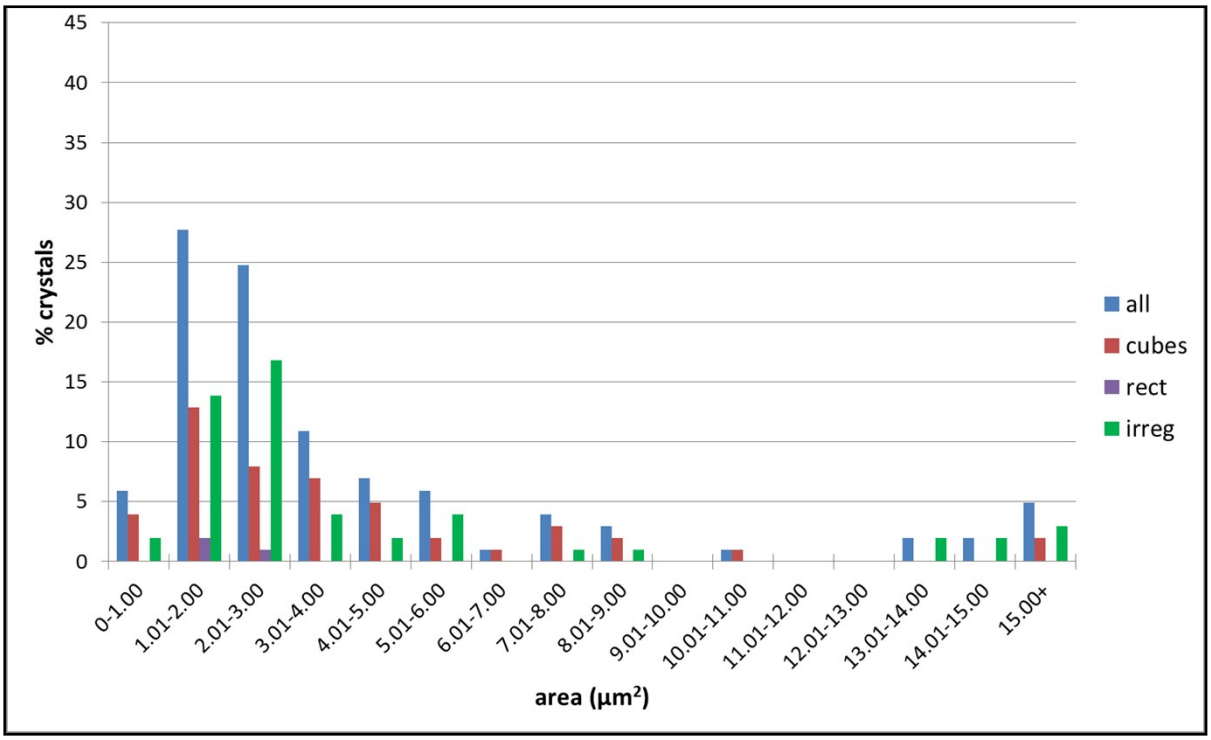

Figure S9: Histogram plot for crystals of MIL-53(Al)*ta* collected from a reaction conducted at a power of 269 ± 2 W and energy of 51.9 kJ mol^{-1}. Crystals are grouped according to size and morphology (key inset).

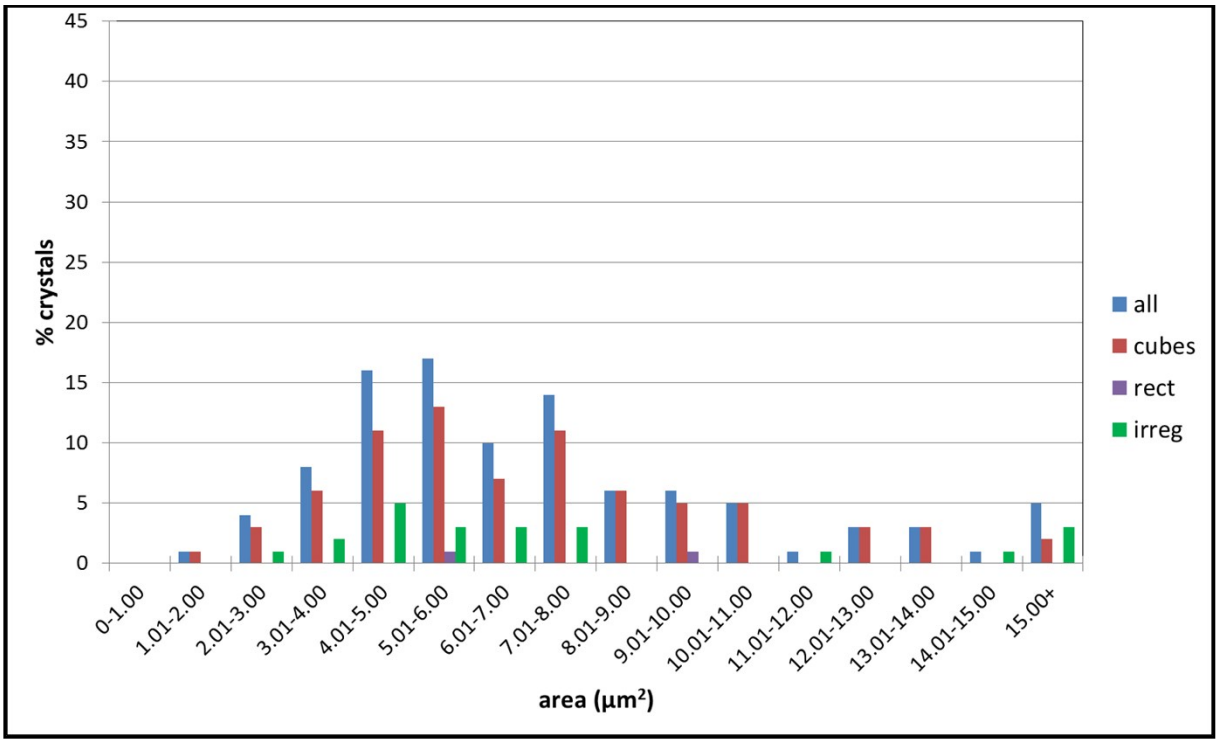

Figure S10: Histogram plot for crystals of MIL-53(Al)*ta* collected from a reaction conducted at a power of 682 ± 4 W and energy of 51.4 kJ mol^{-1}. Crystals are grouped according to size and morphology (key inset).

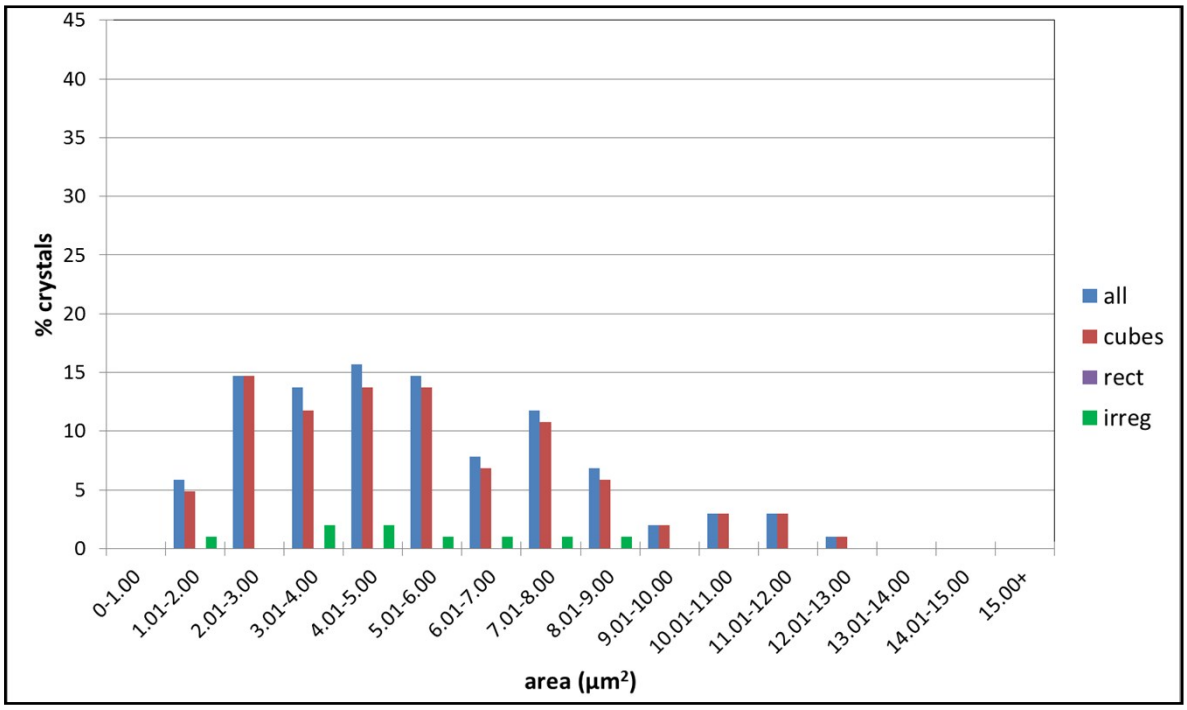

Figure S11: Histogram plot for crystals of MIL-53(Al)*ta* crystals collected from a reaction conducted at a power of 1739 ±44 W and energy of 48.7 kJ mol^{-1}. Crystals are grouped according to size and morphology (key inset).

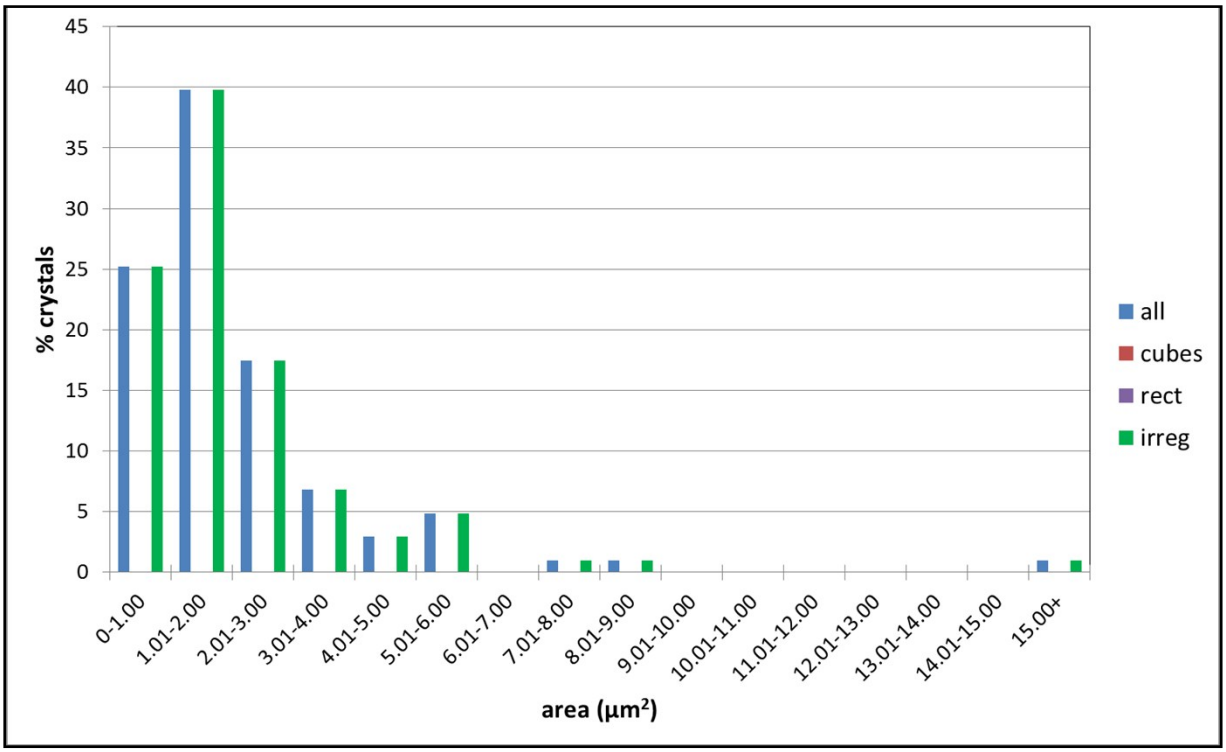

Figure S12: Histogram plot for commercial crystals of Basolite A100. Crystals are grouped according to size and morphology (key inset).

6. Thermogravimetric Analysis (TGA)

TGA were carried out using a Q5000IR analyser (TA Instruments) with an automated vertical overhead thermobalance. Samples of MIL-53(Al)*ta* were heated at a rate of 5 °C/min under N_2 to a maximum of 700 °C. A representative TGA thermograph for MIL-53(Al)*ta* is given in Figure S13 below.

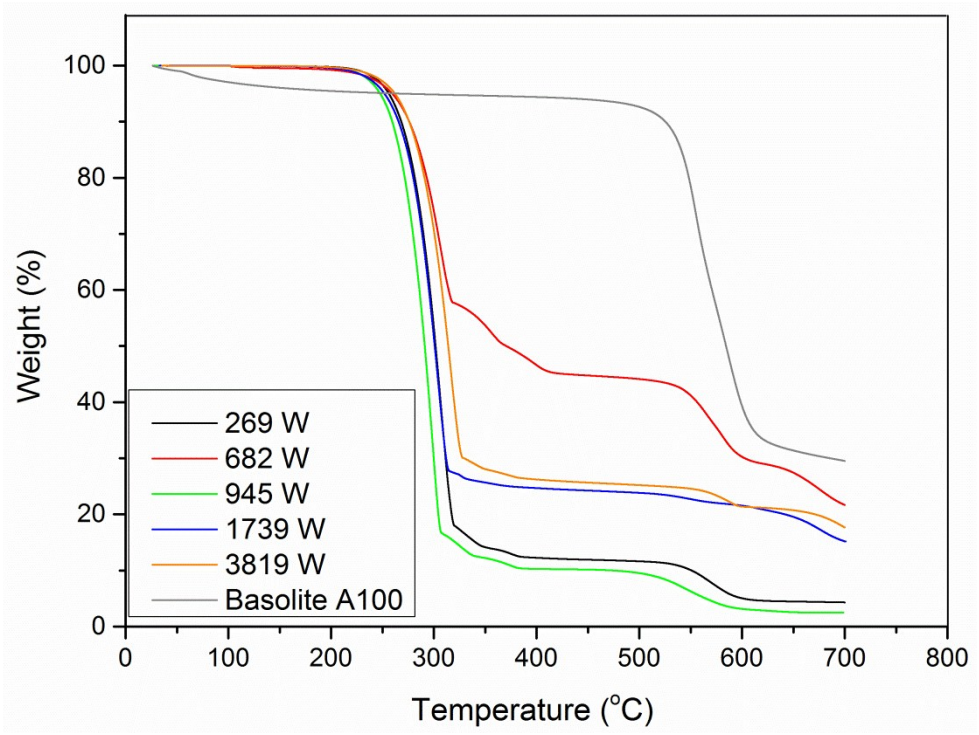

Figure S13: Representative thermographs of MIL-53(Al)*ta* collected from reactions conducted at an energy of *ca.* 51 kJ mol^{-1} and the commercial material (Basolite A100). Legend for the powers inset. All microwave-synthesised materials exhibit three mass losses. The first step between 250 and 300 °C corresponds to un-reacted H_2BDC.[4, 8] The second step between 300 and 350 °C is loss of in pore H_2BDC. [4, 8] The step above 500 °C is loss of coordinated ligand and decomposition of the MOF.[4, 8] Basolite A100 exhibits two mass losses. The first, below 150 °C is loss of physisorbed water.[4, 8] The second mass loss above 500 °C is loss of coordinated ligand and decomposition of the MOF.[4, 8] TGA data suggest that the thermal stabilities of the microwave samples are similar to that of the commercial material as the final decomposition temperatures of all MOF frameworks above are *ca.* 500 °C.

7. Attenuated Total Reflectance Fourier-transformed Infra-red Spectroscopy (ATR FT-IR)

ATR FT-IR spectra were collected using a Fisher Thermo Scientific Nicolet iS5 with iD5-ZnSe ATR attachment and Ominic software. Each spectrum was collected using 16 scans with a data spacing of 0.482 cm^{-1} and a range of 500 to 4000 cm^{-1}.

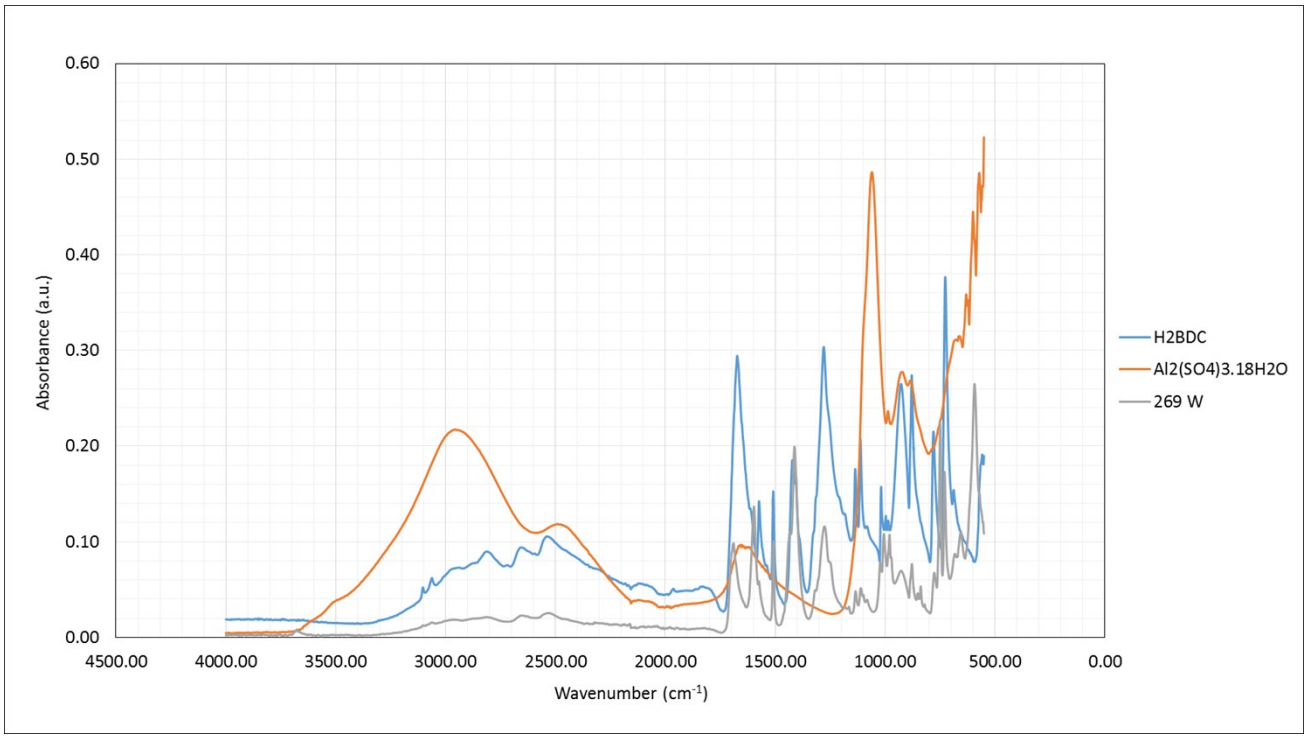

Figure S14: Representative ATR FT-IR spectra of starting materials and MIL-53(Al) recovered from the reaction mixture at 269 W containing both *op* and *ta* phases showing significant overlapping of IR peaks in the region 1250 – 1800 cm^{-1}.

8. References

1. S. Osborne, and Ginnings, *Bureau of Standards Journal of Research,* 1939, **23**, 238 in Handbook of Chemistry and Physics, 53rd ed., Ohio, (1972-1973).
2. P. Datt, *Encyclopedia of Snow, Ice and Glaciers* (Eds.: V. P. Singh, P. Singh, U. K. Haritashya), Springer Netherlands, Dordrecht, 2011, 703.
3. M. Taddei, P. V. Dau, S. M. Cohen, M. Ranocchiari, J. A. van Bokhoven, F. Costantino, S. Sabatini and R. Vivani, *Dalton Trans.,* 2015, **44**, 14019.
4. T. Loiseau, C. Serre, C. Huguenard, G. Fink, F. Taulelle, M. Henry, T. Bataille and G. Férey, *Chem. Eur. J.,* 2004, **10**, 1373.
5. Y.-Y. Liu, K. Leus, M. Grzywa, D. Weinberger, K. Strubbe, H. Vrielinck, R. Van Deun, D. Volkmer, V. Van Speybroeck and P. Van Der Voort, *Eur. J. Inorg. Chem.,* 2012, **16**, 2819.
6. M. Bailey and C. J. Brown, *Acta Cryst.,* 1967, **22**, 387.
7. X. Bokhimi, J. Sánchez-Valente, and F. Pedraza, *J. Solid State Chem.,* 2002, **166**, 182.
8. P. A. Bayliss, I. A. Ibarra, E. Perez, S. Yang, C. C. Tang, M. Poliakoff and M. Schroder, *Green Chem.,* 2014, **16**, 3796.
9. K. S. W. Sing, *Pure Appl. Chem.,* 1982, **54**, 2201.